Microscopic optical potential from chiral nuclear forces

J. W. Holt,[1] N. Kaiser,[2] G. A. Miller,[1] and W. Weise[2,3]
[1]*Physics Department, University of Washington, Seattle, Washington 98195, USA*
[2]*Physik Department, Technische Universität München, D-85747 Garching, Germany*
[3]*ECT*, Villa Tambosi, I-38123 Villazzano (TN), Italy*
(Received 10 April 2013; revised manuscript received 26 July 2013; published 26 August 2013)

The energy- and density-dependent single-particle potential for nucleons is constructed in a medium of infinite isospin-symmetric nuclear matter starting from realistic nuclear interactions derived within the framework of chiral effective field theory. The leading-order terms from both two- and three-nucleon forces give rise to real, energy-independent contributions to the nucleon self-energy. The Hartree-Fock contribution from the two-nucleon force is attractive and strongly momentum dependent, in contrast to the contribution from the three-nucleon force which provides a nearly constant repulsive mean field that grows approximately linearly with the nuclear density. Together, the leading-order perturbative contributions yield an attractive single-particle potential that is however too weak compared to phenomenology. Second-order contributions from two- and three-body forces then provide the additional attraction required to reach the phenomenological depth. The imaginary part of the optical potential, which is positive (negative) for momenta below (above) the Fermi momentum, arises at second order and is nearly inversion-symmetric about the Fermi surface when two-nucleon interactions alone are present. The imaginary part is strongly absorptive and requires the inclusion of an effective mass correction as well as self-consistent single-particle energies to improve agreement with phenomenology.

DOI: 10.1103/PhysRevC.88.024614 PACS number(s): 24.10.Ht, 13.75.Cs, 21.30.−x, 21.65.−f

I. INTRODUCTION

Nuclear optical model potentials provide a highly successful framework for describing nucleon-nucleus scattering across extended regions of the nuclear chart. While local and global phenomenological optical potentials [1–3] have been used to describe total cross sections, elastic scattering angular distributions, and analyzing powers for reactions on target nuclei close to the valley of stability, microscopic optical potentials have no adjustable parameters and may therefore provide the best means for extrapolating to rare isotope reactions that will be studied at the next generation of radioactive beam facilities. Neutron-capture cross sections on exotic, neutron-rich isotopes are particularly relevant for a detailed understanding of heavy-element formation in r-process nucleosynthesis. Although such reactions are experimentally unfeasible in the near future, neutron capture on rare isotopes can be probed indirectly in current and future rare isotope experiments through the (d, p) stripping reaction, a process that is most easily modeled as a three-body problem requiring the nucleon-nucleon potential as well as the nucleon-nucleus optical potential [4] as input.

Phenomenological optical potentials possess several adjustable parameters that characterize the shape of the nuclear density distribution of the target nucleus and vary smoothly with the energy of the projectile and mass number of the target. Microscopic optical potentials, on the other hand, are derived from an underlying model of the nuclear interaction fit to elastic nucleon-nucleon scattering data as well as properties of the lightest nuclei. Within such a microscopic treatment, the optical potential is identified with the nucleon self-energy, a density-dependent complex-valued function given in terms of the nucleon energy and momentum. The nucleon self-energy has been constructed within numerous theoretical frameworks, including Brueckner-Hartree-Fock (BHF) theory [5–11], Dirac-Brueckner-Hartree-Fock (DBHF) theory [12–16], the Green's function formalism [17,18], and chiral perturbation theory [19,20]. The inclusion of three-nucleon forces, while often neglected in microscopic calculations of the optical potential, would seem highly relevant given their importance in achieving nuclear matter saturation at the correct density and binding energy per particle. Recent BHF calculations [21] included effects of the Urbana IX three-nucleon force [22] in a simplified manner [23] and found only a modest improvement in the comparison to elastic scattering data for intermediate-energy scattering of protons from ^{40}C and ^{208}Pb, despite a sizable reduction of the central potential in the dense interior. A more accurate investigation of three-body forces is, however, desirable.

In the present work we make use of the progress that has been achieved in the last decade in constructing high-precision nuclear interactions within the framework of chiral effective field theory. As a first step in the development of microscopic optical potentials capable of describing reactions on rare isotopes, we compute the first- and second-order perturbative contributions to the nucleon self-energy in a medium of isospin-symmetric nuclear matter employing realistic chiral two- and three-nucleon interactions. Extensions to finite nuclei and isospin-asymmetric systems relevant for reactions on nuclei far from the valley of stability will be presented in future work. The resulting optical potentials for infinite nuclear matter can be benchmarked against properties of well-established phenomenological potentials, such as their depth and energy dependence.

We will show that at nuclear matter saturation density $\rho_0 \simeq 0.16\,\mathrm{fm}^{-3}$, the leading-order Hartree-Fock contributions from two- and three-nucleon forces are strongly competitive, with the two-body component significantly attractive and the

three-body component mildly repulsive. Alone they would give rise to a mean field whose depth for a nucleon at vanishing energy (with respect to the Fermi energy) would be $U \simeq -26$ MeV, much smaller than the empirical value of $U \simeq -52$ MeV determined from phenomenological optical model fits to reactions on heavy stable nuclei [3]. Second-order perturbative contributions from two- and three-nucleon forces yield considerable additional attraction of approximately 30 MeV, leading to overall reasonable agreement with phenomenology. The imaginary part, however, turns out to be nearly twice as strong as phenomenological optical potentials at intermediate scattering energies.

The paper is organized as follows. In Sec. II we introduce the relevant formalism and make a connection between the in-medium nucleon self-energy and the nucleon-nucleus optical potential. Explicit formulas are given without any simplifying approximations for the first and second-order perturbative contributions in terms of a partial-wave decomposition of the nucleon-nucleon interaction. We present as well the formulas for the Hartree-Fock contribution to the single-particle potential from the N^{2}LO chiral three-nucleon force. Section III presents the numerical results for the momentum-dependent self-energy associated with negative-energy hole states as well as positive-energy particle states. The impact of second-order three-body forces is then studied by employing a density-dependent nucleon-nucleon potential constructed by summing one nucleon over the filled Fermi sea. Our results for the real and imaginary potential depths as well as their energy dependence is compared to those of phenomenological optical potentials fit to reactions on stable nuclei. We end with a summary and conclusions.

II. MICROSCOPIC OPTICAL MODEL POTENTIALS

A. First- and second-order contributions from two-body forces

In the nuclear optical model, the complicated many-body problem associated with the elastic scattering of a nucleon off a target nucleus is replaced by the more practicable problem of a single nucleon scattering from an equivalent complex mean-field potential:

$$V(\vec{r},\vec{r}\,';E) = U(\vec{r},\vec{r}\,';E) + iW(\vec{r},\vec{r}\,';E), \tag{1}$$

which in general is both nonlocal and energy-dependent. The imaginary part in Eq. (1) accounts for the presence of inelastic scattering, which reduces the total reaction flux in the elastic scattering channel. The simplest phenomenological optical potentials are taken to be local and of Woods-Saxon form in both the real and imaginary components:

$$U(r;E) = \frac{-U_0(E)}{1+e^{(r-R_r)/a_r}}, \quad W(r;E) = \frac{-W_0(E)}{1+e^{(r-R_i)/a_i}}, \tag{2}$$

where the parameters $U_0(E)$, $W_0(E)$, $R_{r,i}$, and $a_{r,i}$ vary smoothly with the mass number A of the nucleus and, in the case of the well-depth parameters U_0 and W_0, also the projectile energy E.

Beyond energies of $E \sim 200$ MeV, this Woods-Saxon form is no longer sufficient, and the real part of the central potential develops a "wine-bottle" shape [3]. Although not relevant for the present calculations in homogeneous isospin-symmetric nuclear matter, phenomenological optical potentials possess real and imaginary spin-orbit terms as well as an imaginary surface term, all of which are proportional to the gradient of the Woods-Saxon distribution [3]. Extensive analysis of the available experimental scattering data yields a real potential well depth $U_0 \simeq 50$–55 MeV for projectile nucleons with very low energies incident on heavy target nuclei. The depth of the imaginary potential vanishes at the Fermi energy and grows to typical values of $W_0 \simeq 10$–12 MeV for projectile energies close to 100 MeV.

Microscopically the optical model potential can be identified with the nucleon self-energy $\Sigma(\vec{r},\vec{r}\,',E)$ in a nucleus [24]. For scattering states with $E > 0$, $\Sigma(\vec{r},\vec{r}\,',E)$ is the nuclear optical potential, while for bound states with $E < 0$, the real part of $\Sigma(\vec{r},\vec{r}\,',E)$ represents the shell model potential. In the present work we consider isospin-symmetric nuclear matter at uniform density $\rho = 2k_f^3/3\pi^2$, in which case it is more appropriate to compute the resulting spin- and isospin-independent self-energy in momentum-space $\Sigma(q,\omega;k_f)$. A local optical model potential for nucleon-nucleus scattering can then be obtained by solving the self-consistent equation for the on-shell energy in terms of the momentum and then folding the resulting density-dependent mean field with a realistic point-nucleon density distribution of the target nucleus. The off-shell dependence of the self-energy $\Sigma(q,\omega;k_f)$ on both q and ω is necessary to describe the nucleon spectral function and nucleon momentum distribution. A complementary work studying the off-shell self-energy, including the effects of three-nucleon forces, is given in Ref. [25].

The first-order Hartree-Fock contribution $\Sigma^{(1)}(q,\omega;k_f)$ to the self-energy from two-body forces is shown diagrammatically in Fig. 1 for states above (1a) and below (1b) the Fermi surface. The Hartree-Fock contribution

$$\Sigma^{(1)}_{2N}(q,\omega;k_f) = \sum_1 \langle \vec{q}\,\vec{h}_1 s s_1 t t_1 | \bar{V}_{2N} | \vec{q}\,\vec{h}_1 s s_1 t t_1 \rangle n_1, \tag{3}$$

is real, ω independent, and changes smoothly as the external momentum q crosses the Fermi surface. In Eq. (3), $\bar{V}_{2N}$ denotes the antisymmetrized potential, $n_1 = \theta(k_f - |\vec{h}_1|)$ is the zero-temperature occupation probability, and the sum is taken over the momentum, spin, and isospin of the intermediate hole state $|\vec{h}_1, s_1, t_1\rangle$. The decomposition of the Hartree-Fock contribution in terms of partial-wave matrix elements of the interaction can be simplified by noting that $\Sigma(q,\omega;k_f)$ is spin and isospin independent when computed for a background medium of isospin-symmetric nuclear matter. Averaging over s and t in Eq. (3) then yields the single-particle potential

$$\begin{aligned} U(q,k_f) &= \frac{1}{2\pi^2}\sum_{lSJT}(2T+1)(2J+1) \\ &\times \int_{\max\{0,(q-k_f)/2\}}^{(q+k_f)/2} dp\, p^2 \min\left\{2, \left(k_f^2-(q-2p)^2\right)/4pq\right\} \\ &\times \langle plSJT|\bar{V}_{2N}|plSJT\rangle, \end{aligned} \tag{4}$$

where $\vec{p} = (\vec{q} - \vec{h}_1)/2$ is the relative momentum of the interacting particles.

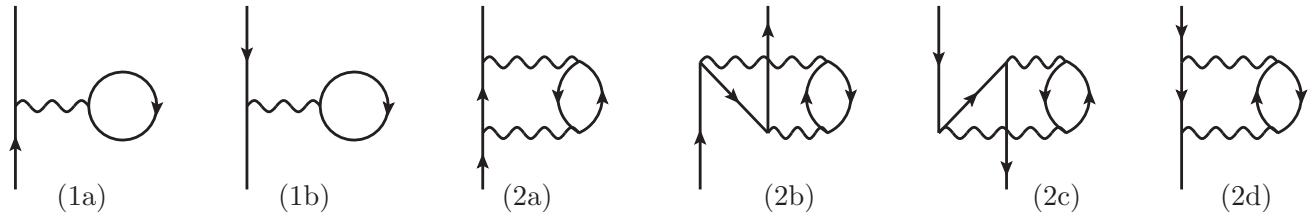

FIG. 1. Diagrams contributing to the nucleon self-energy $\Sigma(q,\omega;k_f)$ at first and second order in perturbation theory from two-body forces. The first-order Hartree-Fock contributions are labeled (1a) and (1b) for particles ($q > k_f$) and holes ($q < kf$), respectively. The second-order contributions to the particle self-energy are labeled (2a) and (2b), while the two contributions to the hole self-energy are labeled (2c) and (2d). The wavy line represents the *antisymmetrized* two-nucleon interaction $\bar{V}_{2N}$, including *direct and exchange* terms.

At second order in perturbation theory, $\Sigma(q,\omega;k_f)$ develops both a real and imaginary part. For particle states above the Fermi surface, there are two distinct contributions labeled (2a) and (2b) in Fig. 1. The contribution (2a) arises from the external particle coupling to a hole state inside the Fermi sea and reads

$$\Sigma^{(2a)}_{2N}(q,\omega;k_f) = \frac{1}{2}\sum_{123}\frac{|\langle \vec{p}_1\vec{p}_3 s_1 s_3 t_1 t_3|\bar{V}_{2N}|\vec{q}\,\vec{h}_2 s s_2 t t_2\rangle|^2}{\omega+\epsilon_2-\epsilon_1-\epsilon_3+i\eta}\bar{n}_1 n_2 \bar{n}_3 (2\pi)^3\delta(\vec{p}_1+\vec{p}_3-\vec{q}-\vec{h}_2), \tag{5}$$

where $\bar{n}_k = 1-n_k$ selects particle states lying above the Fermi momentum. We construct the momentum-dependent mean field by setting $\omega = q^2/(2M_N)$. Fixing $\vec{p}_3$ by momentum conservation, aligning the total momentum $\vec{p}\,' = \vec{p}_1+\vec{p}_3 = \vec{q}+\vec{h}_2$ in the $\vec{e}_z$ direction, and averaging over the external particle spin, isospin and momentum direction then yields the partial-wave decomposition:

$$\begin{aligned} U(q,k_f)+iW(q,k_f) = {} & \frac{8M_N}{(4\pi)^4 q}\sum_{\substack{l_1 l_2 l_3 l_4 J J' M \\ S m_s m_s' T}}(2T+1)\int_{p_a'}^{p_b'}dp'\int_{q_{1a}}^{q_{1b}}dq_1\left[\int_0^{x_0} d\cos\theta_1 \bar{P}_{l_1,m}(\cos\theta_1)\bar{P}_{l_3,m}(\cos\theta_1)\right] \\ & \times\int_{q_{2a}}^{q_{2b}} dq_2\,\bar{P}_{l_2,m'}(\cos\theta_2)\bar{P}_{l_4,m'}(\cos\theta_2)\frac{p' q_1^2 q_2}{(q_2-q_1+i\eta)(q_2+q_1)} i^{l_2+l_3-l_1-l_4} \\ & \times \mathcal{C}^{JM}_{l_1 m S m_s}\mathcal{C}^{JM}_{l_2 m' S m_s'}\mathcal{C}^{J'M}_{l_3 m S m_s}\mathcal{C}^{J'M}_{l_4 m' S m_s'}\langle q_1 l_1 S J T|\bar{V}_{2N}|q_2 l_2 S J T\rangle\langle q_2 l_4 S J' T|\bar{V}_{2N}|q_1 l_3 S J' T\rangle, \end{aligned} \tag{6}$$

where $\vec{q}_1 = (\vec{p}_1-\vec{p}_3)/2$, $\vec{q}_2 = (\vec{q}-\vec{h}_2)/2$, $\bar{P}_{lm}$ is the associated Legendre function P_{lm} multiplied by the factor $\sqrt{(2l+1)(l-m)!/(l+m)!}$, $\cos\theta_2 = (q^2-q_2^2-p'^2/4)/(p'q_2)$, $x_0 = \min\{1,(q_1^2-k_f^2+p'^2/4)/(p'q_1)\}$, and the limits of integration are

$$\begin{aligned} p_a' &= \max\{0, q-k_f\}, \quad p_b' = q+k_f, \\ q_{1a} &= \sqrt{\max\{0, k_f^2-p'^2/4\}}, \quad q_{1b}=\infty, \\ q_{2a} &= |q-p'/2|, \\ q_{2b} &= \min\{\sqrt{(k_f^2+q^2)/2-p'^2/4}, q+p'/2\}. \end{aligned} \tag{7}$$

The expression in Eq. (6) holds also for the hole contribution labeled (2c) in Fig. 1, except that since $q < k_f$ the contribution is purely real and one can drop the $+i\eta$ in the energy denominator.

The diagrams labeled (2b) and (2d) in Fig. 1 are both given by the following expression:

$$\begin{aligned} \Sigma^{(2b)}_{2N}(q,\omega;k_f) = {} & \frac{1}{2}\sum_{123}\frac{|\langle \vec{h}_1\vec{h}_3 s_1 s_3 t_1 t_3|\bar{V}_{2N}|\vec{q}\,\vec{p}_2 s s_2 t t_2\rangle|^2}{\omega+\epsilon_2-\epsilon_1-\epsilon_3-i\eta} \\ & \times n_1\bar{n}_2 n_3(2\pi)^3\delta(\vec{h}_1+\vec{h}_3-\vec{q}-\vec{p}_2). \end{aligned} \tag{8}$$

In contrast to Eq. (5), here the contribution picks up an imaginary part for hole states below the Fermi surface and is purely real for particle states above the Fermi surface. The partial-wave decomposition is very similar to that for $\Sigma^{(2a)}_{2N}(q,\omega;k_f)$, except that $\vec{q}_1 = (\vec{h}_1-\vec{h}_3)/2$, $\vec{q}_2 = (\vec{q}-\vec{p}_2)/2$, and one must make the following replacements:

$$\begin{aligned} +i\eta &\to -i\eta, \quad x_0 \to \min\{1, (k_f^2-q_1^2-p'^2/4)/(p'q_1)\}, \\ p_a' &\to \max\{0, k_f-q\}, \quad p_b' \to 2k_f, \\ q_{1a} &\to 0, \quad q_{1b} \to \sqrt{k_f^2-p'^2/4}, \\ q_{2a} &\to \max\{|q-p'/2|, \sqrt{(k_f^2+q^2)/2-p'^2/4}\}, \\ q_{2b} &\to q+p'/2. \end{aligned} \tag{9}$$

The numerical accuracy of the above formulas for the second-order contributions to the nucleon self energy in nuclear matter has been checked against semianalytic expressions obtained for a simple scalar-isoscalar exchange model of the nuclear force (see the Appendix for details). Although the contributions labeled (2a) and (2c) in Fig. 1 may potentially be divergent, for the scalar-isoscalar exchange interaction all integrals converge. Across a range of momenta and densities we find the agreement between our numerical calculations and the semi-analytical results to be within 1%. The formulas for

iterated one-pion exchange given in Refs. [19,20] have been used as well for checking the partial-wave representation of the second-order contribution.

B. Leading-order contribution from three-body forces

The methods described above for two-body forces can be extended to nuclear many-body forces. For a general three-nucleon force, the first-order Hartree-Fock contribution to the nucleon self-energy is real and energy independent. Summing two of the nucleons over the filled Fermi sea yields

$$\Sigma_{3N}^{(1)}(q,\omega;k_f) = \frac{1}{2}\sum_{12}\langle\vec{q}\,\vec{h}_1\vec{h}_2;ss_1s_2;tt_1t_2|\bar{V}_{3N}|\vec{q}\,\vec{h}_1\vec{h}_2;ss_1s_2;tt_1t_2\rangle n_1n_2, \tag{10}$$

where $\bar{V}_{3N}$ is the fully antisymmetrized three-body interaction.

In the present work we consider only the leading-order N^{2}LO chiral three-nucleon force, which has three terms proportional to the low-energy constants c_1, c_3, c_4, c_D, and c_E. The two-pion exchange component has the momentum-space representation:

$$V_{3N}^{(2\pi)} = \sum_{i\neq j\neq k}\frac{g_A^2}{8f_\pi^4}\frac{\vec{\sigma}_i\cdot\vec{q}_i\,\vec{\sigma}_j\cdot\vec{q}_j}{(\vec{q}_i^{\,2}+m_\pi^2)(\vec{q}_j^{\,2}+m_\pi^2)}F_{ijk}^{\alpha\beta}\tau_i^\alpha\tau_j^\beta, \tag{11}$$

where $g_A = 1.29$, $f_\pi = 92.4$ MeV, $m_\pi = 138$ MeV, and $\vec{q}_i$ is the difference between the final and initial momenta of nucleon i. The isospin tensor

$$F_{ijk}^{\alpha\beta} = \delta^{\alpha\beta}\big(-4c_1m_\pi^2 + 2c_3\vec{q}_i\cdot\vec{q}_j\big) + c_4\epsilon^{\alpha\beta\gamma}\tau_k^\gamma\vec{\sigma}_k\cdot(\vec{q}_i\times\vec{q}_j) \tag{12}$$

results in two terms with the isospin structure $\vec{\tau}_i\cdot\vec{\tau}_j$ and one term proportional to $\vec{\tau}_k\cdot(\vec{\tau}_i\times\vec{\tau}_j)$. The one-pion exchange three-nucleon interaction is proportional to the low-energy constant c_D and given by

$$V_{3N}^{(1\pi)} = -\sum_{i\neq j\neq k}\frac{g_Ac_D}{8f_\pi^4\Lambda_\chi}\frac{\vec{\sigma}_j\cdot\vec{q}_j}{\vec{q}_j^{\,2}+m_\pi^2}\vec{\sigma}_i\cdot\vec{q}_j\,\vec{\tau}_i\cdot\vec{\tau}_j, \tag{13}$$

and finally the chiral three-nucleon contact interaction is proportional to the low-energy constant c_E:

$$V_{3N}^{(\mathrm{ct})} = \sum_{i\neq j\neq k}\frac{c_E}{2f_\pi^4\Lambda_\chi}\vec{\tau}_i\cdot\vec{\tau}_j, \tag{14}$$

where $\Lambda_\chi = 700$ MeV sets the naturalness scale.

In the following, we will employ values of the low-energy constants $c_1 = -0.81\,\mathrm{GeV}^{-1}$, $c_3 = -3.2\,\mathrm{GeV}^{-1}$, and $c_4 = 5.4\,\mathrm{GeV}^{-1}$ for the two-pion exchange three-nucleon force, which can be constrained by nucleon-nucleon elastic scattering phase shifts [26]. The low-energy constants c_D and c_E must be fit to nuclear systems with $A \geqslant 3$. We employ the values $c_D = -0.20$ and $c_E = -0.205$ extracted from a fit [27] to the binding energies of $A = 3$ nuclei and the half-life of ^{3}H. In fact, the relevant dimensionful low-energy constants are $C_D = c_D/\Lambda_\chi$ and $C_E = c_E/\Lambda_\chi$ with values $C_D \simeq C_E \simeq -0.3\ \mathrm{GeV}^{-1}$.

In Fig. 2 we show the diagrammatic contributions to the nucleon self-energy arising from the leading-order chiral three-nucleon force. The direct Hartree diagrams, labeled as (a) and (b) in Fig. 2, of the chiral two-pion exchange three-nucleon force are non-vanishing only for the terms proportional to the low-energy constants c_1 and c_3. The sum of these two diagrams gives

$$U(q,k_f) = \frac{g_A^2m_\pi^6}{(2\pi f_\pi)^4}\Bigg\{14(c_3-c_1)u^4 + (3c_1-2c_3)u^2 - 4c_3u^6 + (12c_1-10c_3)u^3[\arctan 2u + \arctan(u+x) + \arctan(u-x)] + \left[\frac{c_3}{2}(1+9u^2) - \frac{3c_1}{4}(1+8u^2)\right]\ln(1+4u^2) + \frac{u^3}{x}[3c_3-4c_1+2(c_1-c_3)(x^2-u^2)]\ln\frac{1+(u+x)^2}{1+(u-x)^2}\Bigg\}, \tag{15}$$

where $u = k_f/m_\pi$ and $x = q/m_\pi$.

The Fock diagrams, labeled as (c) and (d) in Fig. 2 are nonvanishing for all terms in the two-pion exchange three-nucleon force:

$$U(q,k_f) = \frac{g_A^2m_\pi^6}{(4\pi f_\pi)^4x^2}\Bigg\{3c_1H^2(x,u) + \left(\frac{c_3}{2}-c_4\right)G_S^2(x,u) + (c_3+c_4)G_T^2(x,u) + \int_0^u d\xi\Bigg[6c_1H(\xi,u)\frac{\partial H(\xi,x)}{\partial x} + (c_3-2c_4)G_S(\xi,u)\frac{\partial G_S(\xi,x)}{\partial x} + 2(c_3+c_4)G_T(\xi,u)\frac{\partial G_T(\xi,x)}{\partial x}\Bigg]\Bigg\}, \tag{16}$$

with the auxiliary functions:

$$H(x,u) = u(1+x^2+u^2) - \frac{1}{4x}[1+(u+x)^2][1+(u-x)^2]\ln\frac{1+(u+x)^2}{1+(u-x)^2}, \tag{17}$$

$$G_S(x,u) = \frac{4ux}{3}(2u^2-3) + 4x[\arctan(u+x) + \arctan(u-x)] + (x^2-u^2-1)\ln\frac{1+(u+x)^2}{1+(u-x)^2}, \tag{18}$$

$$G_T(x,u) = \frac{ux}{6}(8u^2+3x^2) - \frac{u}{2x}(1+u^2)^2 + \frac{1}{8}\left[\frac{(1+u^2)^3}{x^2} - x^4 + (1-3u^2)(1+u^2-x^2)\right]\ln\frac{1+(u+x)^2}{1+(u-x)^2}. \tag{19}$$

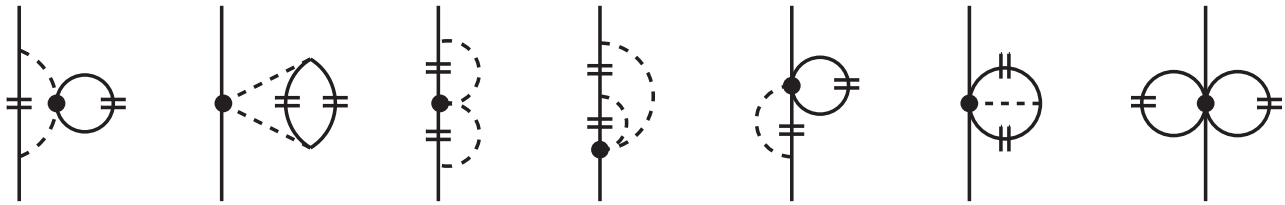

FIG. 2. Diagrammatic contributions from the N^{2}LO chiral three-nucleon force to the optical potential at first order in perturbation theory. The large dots represent vertices proportional to the low-energy constants c_1, c_3, c_4, c_D, and c_E, while the short double-lines indicate a medium insertion $-2\pi\delta(k_0)\theta(k_f - |\vec{k}|)$. The external line can be either a hole or particle state. Reflected diagrams of (d) and (e) are not shown.

As shown in Sec. III, the sum of the Hartree and Fock contributions from the two-pion exchange three-nucleon force gives rise to a significantly repulsive mean field. The Hartree term is approximately 75% larger in magnitude and of opposite sign as the attractive Fock term.

The contribution to the single-particle potential arising from the one-pion exchange three-nucleon force, proportional to c_D, is given by

$$U(q,k_f) = \frac{g_A c_D m_\pi^6}{(2\pi f_\pi)^4 \Lambda_\chi}\left\{u^6 - \frac{7u^4}{4} + \frac{u^2}{8} - \frac{1+12u^2}{32}\ln(1+4u^2) + u^3[\arctan 2u + \arctan(u+x) + \arctan(u-x)] + \frac{u^3}{4x}(x^2-u^2-1)\ln\frac{1+(u+x)^2}{1+(u-x)^2}\right\}, \tag{20}$$

which depends very weakly on the momentum q and is attractive for $c_D < 0$. The first-order contribution from the N^{2}LO contact interaction is independent of the external momentum and has the form

$$U(q,k_f) = -\frac{c_E k_f^6}{4\pi^4 f_\pi^4 \Lambda_\chi}, \tag{21}$$

which is of course repulsive for $c_E < 0$. As we will find in Sec. III, together $V_{3N}^{1\pi}$ and $V_{3N}^{\rm ct}$ provide a nearly constant repulsive mean field.

The above analytical expressions result from an exact calculation of the Hartree-Fock contribution to the nuclear mean field. To include second-order corrections from three-nucleon forces, we compute the expressions in Eqs. (5) and (8) using a density-dependent two-body effective interaction [28–30].

III. RESULTS

In the present section we employ the N^{3}LO chiral two-body interaction of Ref. [26] together with the N^{2}LO chiral three-body interaction with low-energy constants given in Sec. II to compute the contributions to the nuclear optical potential up to second order in perturbation theory. In addition we perform calculations of the single-particle energy also for hole states with $q < k_f$. We are particularly interested in comparisons of our microscopic optical potential to local phenomenological potentials and in the effects from three-nucleon forces, which until now have been treated only approximately in several complementary studies [21,25].

In Fig. 3 we plot the real part of the on-shell self-energy $[\omega = q^2/(2M_N)]$ as a function of momentum and density. The advantage in using the free-particle spectrum is that various general identities, such as the Hugenholtz–Van-Hove and Luttinger theorems [33,34]

$$\frac{k_f^2}{2M_N} + U(k_f,k_f) = \bar{E}(k_f) + \frac{k_f}{3}\frac{\partial \bar{E}(k_f)}{\partial k_f}, \qquad W(q,k_f) = C\,|k_f - q|(k_f - q) + \cdots \tag{22}$$

are automatically fulfilled when the relevant quantities are computed to a particular order in perturbation theory. The thick solid line denotes the Hartree-Fock contribution from two-body forces, and the vertical dotted lines show the Fermi momentum corresponding to the densities $\rho = \{0.2\rho_0, 0.4\rho_0, 0.6\rho_0, 0.8\rho_0, 0.9\rho_0, \rho_0\}$ from the upper left corner to the bottom right, where $\rho_0 \simeq 0.16$ fm^{-3}. The Hartree-Fock term has a nearly parabolic form, and when summed with the free-particle kinetic energy $q^2/(2M_N)$ it can be well approximated as [31]

$$\epsilon_q = \frac{q^2}{2M^*} + \Delta, \tag{23}$$

where M^* is the effective mass and the energy shift Δ is independent of momentum. In Fig. 3 the momenta are taken up to $q = 2.5$ fm^{-1}, which, for all the densities considered here, corresponds to possible two-particle relative momenta well below the cutoff of $\Lambda \simeq 2.5$ fm^{-1}.

The Hartree-Fock three-body force contribution exhibits a very weak momentum dependence that gives rise to only a small decrease in the effective mass at the Fermi surface [32]. The strength of the mean field from chiral three-nucleon forces increases nearly linearly with the density of the medium. At saturation density it gives a repulsive contribution of approximately 20 MeV. In Fig. 4 we plot separately the mean fields associated with the different contributions $V_{3N}^{2\pi}$, $V_{3N}^{1\pi}$, and $V_{3N}^{\rm ct}$ at nuclear matter saturation density, corresponding

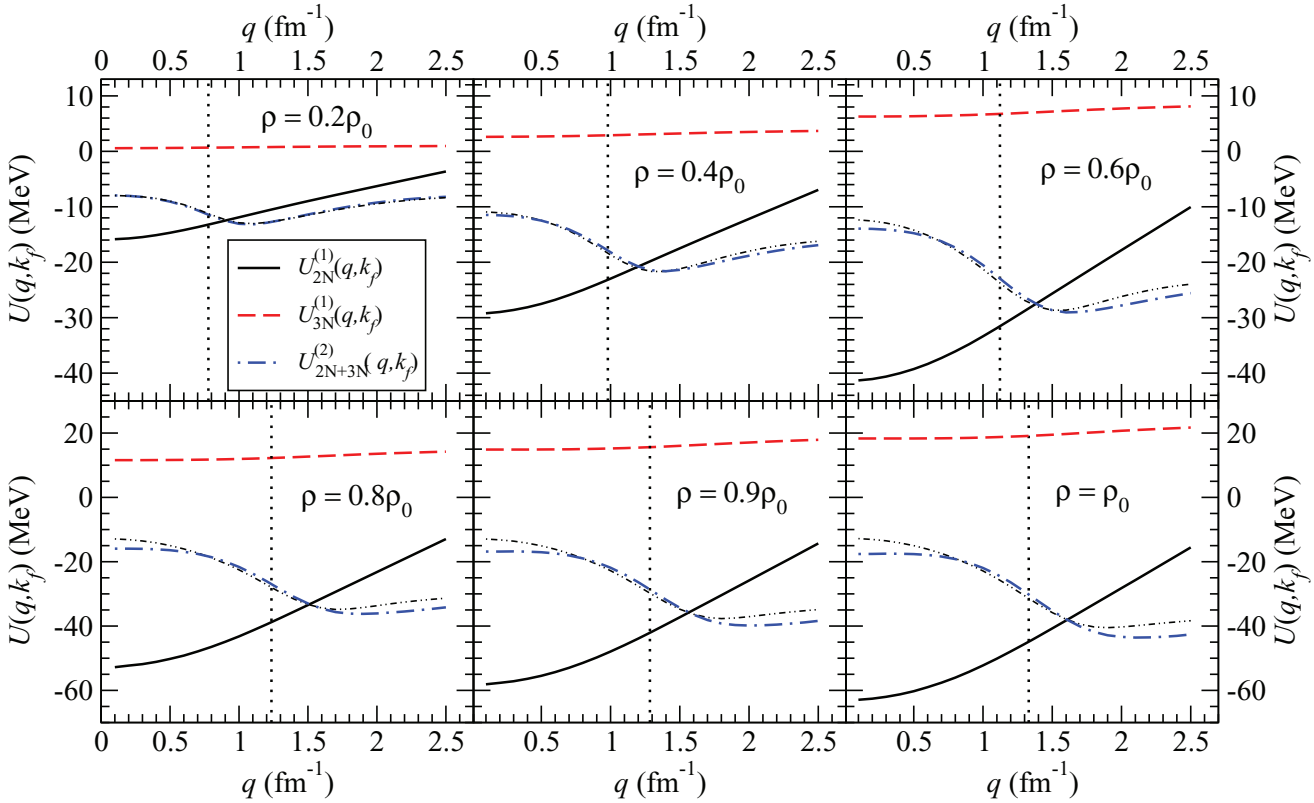

FIG. 3. (Color online) Contributions to the real part of the momentum- and density-dependent single-particle potential. The solid and dashed-double-dotted lines are the first- and second-order contributions, respectively, from the N^{3}LO chiral two-body potential, while the dashed line is the first-order contribution from the N^{2}LO chiral three-nucleon force. The vertical dotted line denotes the Fermi momentum, and the dashed-dotted line is the second-order contribution with three-body forces. The results are shown for the case $\omega = q^2/(2M_N)$.

to $k_f = 1.33$ fm^{-1}. The 2π-exchange chiral three-nucleon force provides much of the observed repulsion from three-body forces and accounts also for most of the momentum dependence, which arises primarily for momenta above the Fermi surface. The 1π and contact interactions together give rise to a small net repulsive mean field that is nearly momentum independent. For nucleon-nucleus scattering, it therefore appears that the low-energy constants c_D and c_E

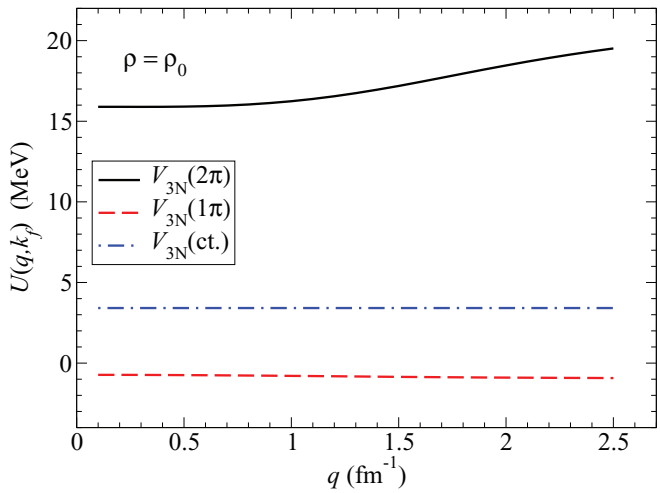

FIG. 4. (Color online) Hartree-Fock contributions to the real part of the nuclear single-particle potential from chiral three nucleon forces. The two-pion exchange, one-pion exchange, and contact three-nucleon force contributions are evaluated from Eqs. (15)–(21) and plotted separately as a function of the momentum.

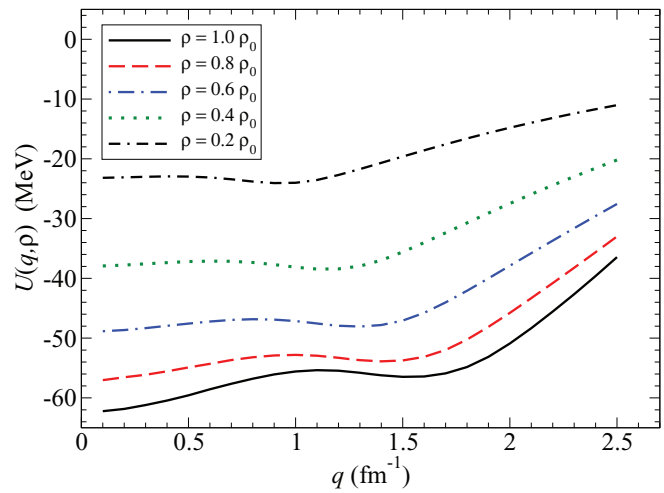

FIG. 5. (Color online) The real part of the momentum-dependent single-particle potential at second order in perturbation theory from chiral two- and three-nucleon forces. The potential is computed for a medium of symmetric nuclear matter at densities ranging from $0.2\rho_0$ to ρ_0.

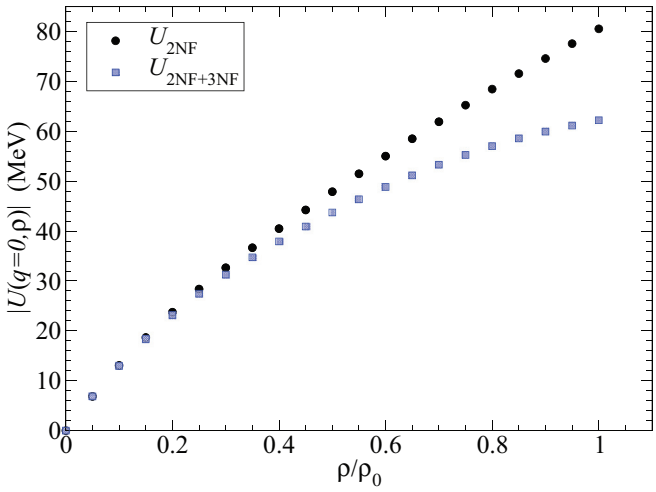

FIG. 6. (Color online) Density dependence of the real part of the single-particle potential at zero momentum from second order perturbation theory. Results for two-nucleon forces alone as well as for the sum of two- and three-nucleon forces are shown.

are strongly correlated, with variations along the line

$$c_E = \alpha \cdot c_D + \text{const} \tag{24}$$

giving nearly equivalent descriptions of the mean field, where the constant of proportionality $\alpha \simeq 0.21 \pm 0.02$ is weakly dependent on momentum and density. Inspection of Eq. (21) reveals that in the chiral limit only the leading k_f^6 term survives, and the correlation coefficient would be $\alpha = g_A/4 \simeq 0.3$.

The second-order contributions to the single-particle energy are shown as the dashed-dotted lines in Fig. 3. Below the Fermi surface, they have a momentum dependence that is nearly opposite to that of the Hartree-Fock contribution, giving rise to a quasiparticle effective mass at the Fermi surface that is close to the mass in vacuum [31]. In Fig. 3 we plot also the second-order contribution without three-nucleon forces, denoted by the dashed-double-dotted line. Despite the fact that the three-nucleon force gives rise to substantial repulsion at the Hartree-Fock approximation, it appears that second-order effects are quite small and produce additional attraction at both low and high momenta.

The combined real part of the nucleon self-energy is shown in Fig. 5 as a function of density and momentum. We note that for low to moderate densities, the single-particle potential for states with momenta $q < k_f$ is nearly constant, but in the vicinity of the saturation density, three-nucleon forces at second-order introduce additional attraction for low values of q. The well depth at $q = 0$ as a function of density is shown in Fig. 6 for two-nucleon forces alone as well as for combined two- and three-body forces. Three-nucleon forces become relevant at about 40% of nuclear matter saturation density and result in a potential that is significantly nonlinear in the density.

We plot in Fig. 7 the imaginary part of the nucleon self-energy arising from the second-order perturbative

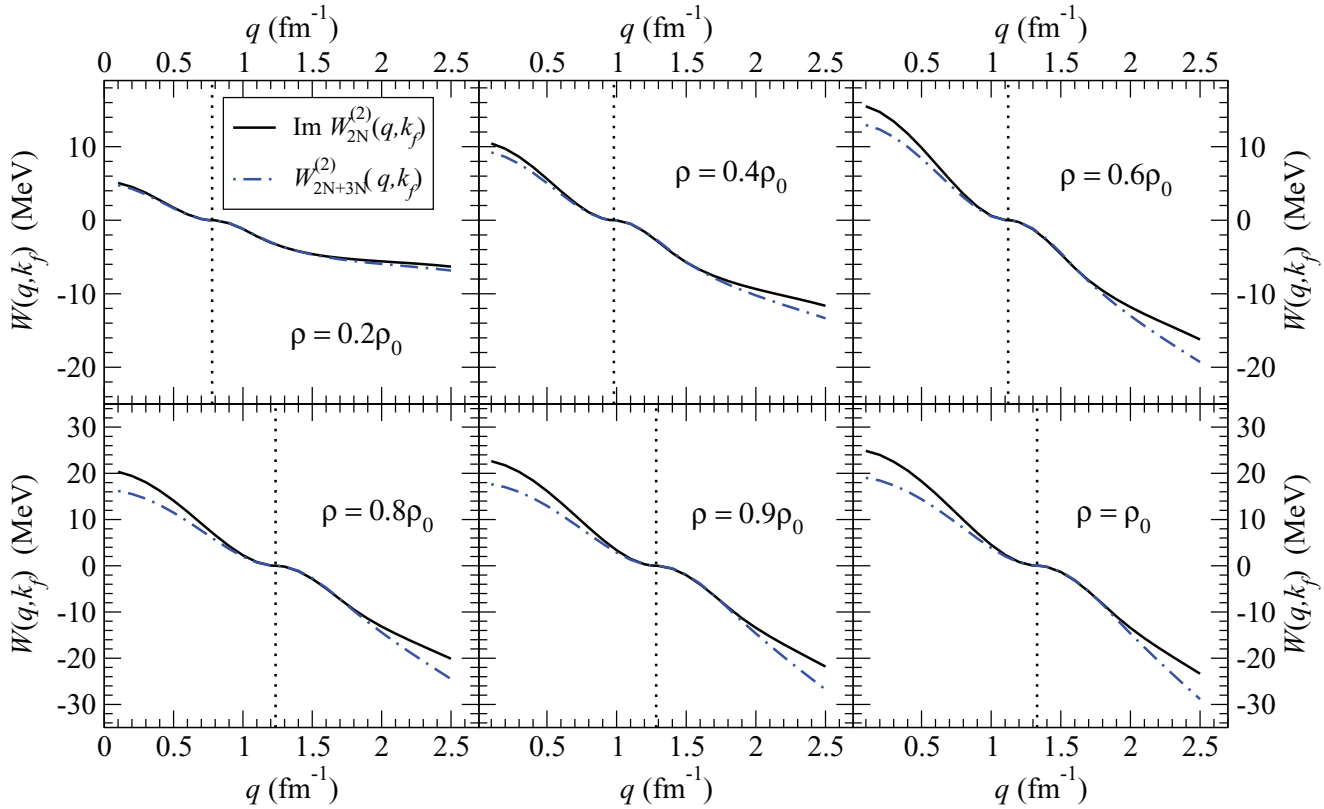

FIG. 7. (Color online) The imaginary part of the momentum- and density-dependent optical potential arising from chiral two- and three-nucleon forces iterated to second order. The vertical dotted line denotes the Fermi momentum.

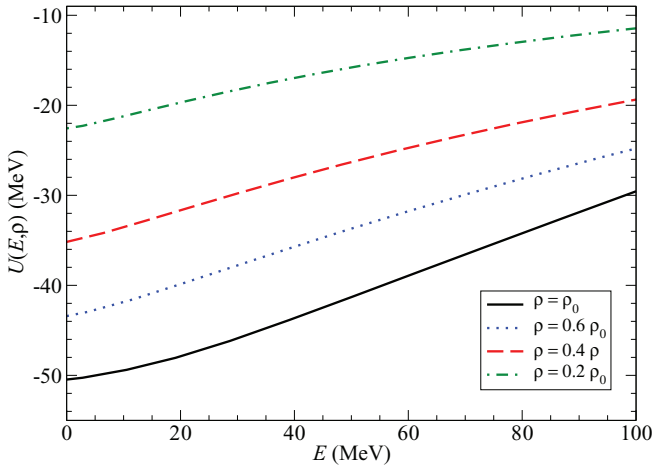

FIG. 8. (Color online) The real part of the energy-dependent optical potential at second order in perturbation theory from chiral two- and three-nucleon forces for several values of the nuclear density.

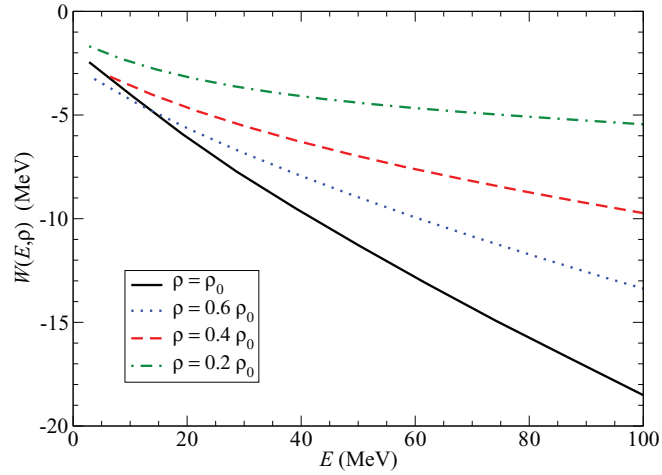

FIG. 9. (Color online) The imaginary part of the energy-dependent optical potential at second order in perturbation theory from chiral two- and three-nucleon forces for several values of the nuclear density.

contributions (both with and without three-nucleon forces) as a function of momentum and density. In agreement with Luttinger's theorem [34] the imaginary part vanishes quadratically in the vicinity of the Fermi surface above and below k_f for both two- and three-nucleon force contributions. Omitting the chiral three-body force, we find that the imaginary part is approximately inversion-symmetric about the Fermi momentum, $W(q, k_f) \simeq -W(2k_f - q, k_f)$, a property which is often assumed in the dispersion optical model formalism [35]. This feature is, however, modified with the inclusion of three-nucleon forces, which provide an attractive contribution at both very low and very high momenta.

The real and imaginary parts of the nuclear optical potential are obtained by solving the self-consistent equation for the momentum $q(E)$ as a function of the energy [36–38]:

$$\begin{aligned} E(q) &= \frac{q^2}{2M_N} + \mathrm{Re}\,\Sigma(q, E(q); k_f), \\ U(E,\rho) &= \mathrm{Re}\,\Sigma(q(E), E; k_f), \\ W(E,\rho) &= \left(1 + \frac{M_N}{q}\frac{\partial U}{\partial q}\right)^{-1} \mathrm{Im}\,\Sigma(q(E), E; k_f). \end{aligned} \tag{25}$$

Such a prescription reduces the second-order contributions due to the larger energy difference between particle and hole states in the energy denominators. In solving for the self-consistent energies, we employ the effective mass plus energy shift parametrization in Eq. (23). The resulting real and imaginary parts of the optical potential are shown in Figs. 8 and 9 for several nuclear densities as a function of the energy E. We have restricted the presentation to positive energies $E > 0$, which start from a value already higher than the Fermi energy. The well depth of the real potential for a scattering state at zero incident energy is approximately 50 MeV, which is in very good agreement with the phenomenological depth of 50–55 MeV, but the energy dependence is slightly weaker than that of phenomenological potentials [3].

The overall strength of the imaginary potential at nuclear matter saturation density for an intermediate scattering energy of $E \simeq 100$ MeV is approximately 18 MeV, which would seem too large compared to the empirical value, $|W| \simeq 10$–12 MeV [3]. This large magnitude of the imaginary part of the optical potential is a feature shared by many microscopic calculations. Already second-order one-pion exchange gives rise to quantitatively similar results (see Fig. 6 in Ref. [20]). One should recall, however, that the phenomenological absorptive strength $|W|$ is reduced for finite nuclei, which have a characteristic gap in the single-particle energy spectrum around the Fermi energy. The nuclear matter calculation does not feature such a gap at the Fermi surface so that there is an increased phase space open for absorptive processes, leading to an overestimate of $|W|$.

IV. CONCLUSIONS

We have performed a microscopic calculation of the on-shell self-energy of a nucleon in a medium of isospin-symmetric nuclear matter at uniform density ρ up to second order in many-body perturbation theory. The starting point is a realistic N^{3}LO chiral two-nucleon potential supplemented with the N^{2}LO chiral three-nucleon force. The first- and second-order contributions from two-body forces are attractive, but below the Fermi momentum they have an opposite dependence on the momentum. The N^{2}LO chiral three-body force is found to provide substantial repulsion that grows slowly with momentum and nearly linearly with the density. Summing up all of these contributions, the resulting real part of the microscopic optical potential agrees qualitatively with the depth of phenomenological optical potentials. The absorptive strength of the imaginary part of the potential calculated in nuclear matter is considerably larger than the empirical one deduced for finite nuclei. This suggests that the inclusion of an energy gap at the Fermi surface may be necessary in order to achieve a successful description of nucleon-nucleus scattering at low to intermediate energies. In the future we plan to extend our calculations to finite nuclei and isospin-asymmetric nuclear matter that will be important

to describe neutron-capture cross sections on neutron-rich isotopes.

ACKNOWLEDGMENTS

Work supported in part by BMBF, the DFG cluster of excellence Origin and Structure of the Universe, by the DFG, NSFC (CRC110), and US DOE Grant No. DE-FG02-97ER-41014.

APPENDIX: NUCLEAR OPTICAL POTENTIAL FROM SECOND-ORDER SCALAR-ISOSCALAR BOSON EXCHANGE

As a benchmark for our involved numerical calculations of the nuclear mean field at second order in perturbation theory, we derive exact semianalytical expressions for the on-shell self-energy arising from scalar-isoscalar boson exchange. The attractive central NN potential in momentum space is given by

$$V_C(Q) = -\frac{g^2}{m^2+Q^2}\,, \tag{A1}$$

with g the coupling constant, m the boson mass, and Q the momentum transfer between the two nucleons.

The first-order contribution to the real part of the optical potential for states both above ($q > k_f$) and below ($q < k_f$) the Fermi surface reads

$$U(q,k_f)^{(1)} = \frac{g^2 m}{4\pi^2}\left\{ -\arctan(u+x) - \arctan(u-x) + u - \frac{8u^3}{3} + \frac{1+u^2-x^2}{4x}\ln\frac{1+(u+x)^2}{1+(u-x)^2}\right\}, \tag{A2}$$

with abbreviations $u = k_f/m$ and $x = q/m$.

Due to the presence of poles in Fermi sphere integrals, the analytic expression of the second-order contributions cannot be continued directly from below to above the Fermi surface. We therefore distinguish the contributions to the optical potential for momenta $q < k_f$ and $q > k_f$. Setting $\omega = q^2/(2M_N)$, the complex-valued mean field $U(q,k_f) + i\,W(q,k_f)$ inside the Fermi sphere $q < k_f$ is given by the sum of the following contributions (in these expressions the superscript "H" and "F" refer to Hartree and Fock diagrams, and the subscript denotes the number of medium insertions [19]):

$$U_2(q,k_f)^{(H)} = \frac{g^4 M_N}{8\pi^3}\left\{ \arctan(u+x) + \arctan(u-x) - u + \frac{x^2-u^2-1}{4x}\ln\frac{1+(u+x)^2}{1+(u-x)^2}\right\}, \tag{A3}$$

$$U_2(q,k_f)^{(F)} = \frac{g^4 M_N}{16\pi^3}\left\{ \int_0^{(u-x)/2} d\xi\, 8\xi + \int_{(u-x)/2}^{(u+x)/2} d\xi\,\frac{1}{x}[u^2-(2\xi-x)^2]\right\}\frac{\arctan 2\xi - \arctan\xi}{1+2\xi^2}\,, \tag{A4}$$

$$U_3(q,k_f)^{(H)} = \frac{g^4 M_N}{8\pi^4}\int_{-1}^{1} dy\left\{\left[uxy + \frac{1}{2}(u^2-x^2y^2)\ln\frac{u+xy}{u-xy}\right]\frac{s^2}{1+s^2} + \int_{-xy}^{s-xy} d\xi\left[2u\xi + (u^2-\xi^2)\ln\frac{u+\xi}{u-\xi}\right] \times \frac{xy+\xi}{[1+(xy+\xi)^2]^2} + \frac{1}{x}\int_0^u d\xi\,\frac{\xi^2\sigma^2}{1+\sigma^2}\ln\frac{|x+\xi y|}{|x-\xi y|}\right\}, \tag{A5}$$

with auxiliary functions $s = xy + \sqrt{u^2-x^2+x^2y^2}$ and $\sigma = \xi y + \sqrt{u^2-\xi^2+\xi^2y^2}$:

$$U_3(q,k_f)^{(F)} = \frac{g^4 M_N}{16\pi^4}\int_{-1}^{1} dy\left\{\int_0^u d\xi\,\frac{\xi^2}{xR}\ln(1+\sigma^2)\ln\frac{|xR+(x^2-\xi^2-1)y\xi|}{|xR+(1+\xi^2-x^2)y\xi|} - \int_{-1}^{1} dz\,\frac{yz\,\theta(y^2+z^2-1)}{4|yz|\sqrt{y^2+z^2-1}}\ln(1+s^2)\ln(1+t^2)\right\}, \tag{A6}$$

with auxiliary functions $t = xz + \sqrt{u^2-x^2+x^2z^2}$ and $R = \sqrt{(1+x^2-\xi^2)^2+4\xi^2(1-y^2)}$:

$$W_2(q,k_f)^{(H)} = \frac{g^4 M_N}{16\pi^3}\left\{\ln[1+(u+x)^2] + \ln[1+(u-x)^2] - 2(1+u^2) + \frac{2x^2}{3} + \frac{1+u^2-x^2}{x}[\arctan(u+x) - \arctan(u-x)]\right\} \tag{A7}$$

$$W_2(q,k_f)^{(F)} = \frac{g^4 M_N}{32\pi^3}\left\{\int_0^{(u-x)/2} d\xi\, 8\xi + \int_{(u-x)/2}^{(u+x)/2} d\xi\,\frac{1}{x}[u^2-(2\xi-x)^2]\right\}\frac{\ln(1+4\xi^2)}{1+2\xi^2}\,, \tag{A8}$$

$$W_3(q,k_f)^{(H)} = \frac{g^4 M_N}{16\pi^3}\int_{-1}^{1} dy\left\{(1+2u^2-2x^2y^2)\frac{s^2}{1+s^2} - \ln(1+s^2) + 2xy\left(\arctan s - \frac{s}{1+s^2}\right) + \int_0^u d\xi\,\frac{2\xi^2}{x}\,\theta(x-\xi|y|)\frac{\sigma^2}{1+\sigma^2}\right\}, \tag{A9}$$

$$W_3(q,k_f)^{(F)} = \frac{g^4 M_N}{16\pi^3}\int_{-1}^{1} dy\left\{-\int_{-1}^{1} dz\,\ln(1+s^2)\ln(1+t^2)\frac{\theta(1-y^2-z^2)}{4\pi\sqrt{1-y^2-z^2}} - \int_0^u d\xi\,\frac{\xi^2}{xR}\,\theta(x-\xi|y|)\ln(1+\sigma^2)\right\}, \tag{A10}$$

$$W_4(q,k_f)^{(H)} = \frac{g^4 M_N}{8\pi^3}\left\{\frac{2x^2}{3} - 2u^2 - \frac{1}{2} - \ln(1+4x^2) + \frac{4x^2-3}{4x}\arctan 2x + \int_{-1}^{1} dy\left[\frac{1+u^2-x^2y^2}{1+s^2} + 2xy\left(\frac{s}{1+s^2} - \arctan s\right) + \ln(1+s^2)\right]\right\}, \tag{A11}$$

$$W_4(q,k_f)^{(F)} = \frac{g^4 M_N}{16\pi^3}\int_{-1}^{1} dy\int_0^u d\xi\,\frac{\xi^2}{xR}\big[\theta(x-\xi|y|)\theta(\xi-x)\ln(1+\sigma^2) + \theta(x-\xi)\ln\big(1+\sigma_x^2\big)\big], \tag{A12}$$

with $\sigma_x = \xi y + \sqrt{u^2 - x^2 + \xi^2 y^2}$.

Similarly, the second-order contributions to $U(q,k_f) + i\,W(q,k_f)$ for momenta outside the Fermi sphere $q > k_f$ are given by

$$U_2(q,k_f)^{(H)} = \frac{g^4 M_N}{8\pi^3}\left\{\arctan(u+x) - \arctan(x-u) - u + \frac{x^2-u^2-1}{4x}\ln\frac{1+(u+x)^2}{1+(u-x)^2}\right\}, \tag{A13}$$

$$U_2(q,k_f)^{(F)} = \frac{g^4 M_N}{16\pi^3 x}\int_{(x-u)/2}^{(u+x)/2} d\xi\,[u^2-(2\xi-x)^2]\frac{\arctan 2\xi - \arctan\xi}{1+2\xi^2}, \tag{A14}$$

$$U_3(q,k_f)^{(H)} = \frac{g^4 M_N}{8\pi^4}\left\{\int_{y_{\min}}^{1} dy\left\{\left[uxy + \frac{1}{2}(u^2-x^2y^2)\ln\frac{u+xy}{|u-xy|}\right]\mathcal{A}_y\left[\frac{s^2}{1+s^2}\right] + \int_{xy-s}^{s-xy} d\xi\left[2u\xi + (u^2-\xi^2)\ln\frac{u+\xi}{u-\xi}\right]\frac{xy+\xi}{[1+(xy+\xi)^2]^2}\right\} + \frac{1}{x}\int_{-1}^{1} dy\int_0^u d\xi\,\frac{\xi^2\sigma^2}{1+\sigma^2}\ln\frac{x+\xi y}{x-\xi y}\right\}, \tag{A15}$$

with $y_{\min} = \sqrt{1-u^2/x^2}$ and the antisymmetrization prescription $\mathcal{A}_y[f(y)] = f(y) - f(-y)$:

$$U_3(q,k_f)^{(F)} = \frac{g^4 M_N}{16\pi^4}\left\{-\int_{y_{\min}}^{1} dy\int_{y_{\min}}^{1} dz\,\mathcal{A}_y[\ln(1+s^2)]\mathcal{A}_z[\ln(1+t^2)]\frac{\theta(y^2+z^2-1)}{4\sqrt{y^2+z^2-1}} + \int_{-1}^{1} dy\int_0^u d\xi\,\frac{\xi^2}{xR} \times \ln(1+\sigma^2)\ln\frac{xR+(x^2-\xi^2-1)y\xi}{xR+(1+\xi^2-x^2)y\xi}\right\}, \tag{A16}$$

$$W_2(q,k_f)^{(H)} = \frac{g^4 M_N}{16\pi^3}\left\{\ln\frac{1+(u+x)^2}{1+(u-x)^2} - \frac{2u}{3x}(3+2u^2) + \frac{1+u^2-x^2}{x}[\arctan(u+x) - \arctan(x-u)]\right\}, \tag{A17}$$

$$W_2(q,k_f)^{(F)} = \frac{g^4 M_N}{32\pi^3 x}\int_{(x-u)/2}^{(u+x)/2} d\xi\,[u^2-(2\xi-x)^2]\frac{\ln(1+4\xi^2)}{1+2\xi^2}, \tag{A18}$$

$$W_{34}(q,k_f)^{(H)} = \frac{g^4 M_N}{16\pi^3}\left\{\frac{1}{x}\left[\frac{u}{2} + \frac{4u^3}{3} - \frac{1}{4}(1+4u^2)\arctan 2u\right] + \theta(\sqrt{2}u-x)\int_{y_{\min}}^{u/x} dy\,(x^2y^2-u^2)\mathcal{A}_y\left[\frac{s^2}{1+s^2}\right] + \int_{y_{\min}}^{1} dy\,\mathcal{A}_y\left[-\ln(1+s^2) + \frac{s^2}{1+s^2}(1+u^2-x^2y^2) + 2xy\left(\arctan s - \frac{s}{1+s^2}\right)\right]\right\}, \tag{A19}$$

$$W_{34}(q,k_f)^{(F)} = \frac{g^4 M_N}{16\pi^3}\left\{\frac{\theta(\sqrt{2}u-x)}{4\pi}\int_{y_{\min}}^{1} dy\int_{y_{\min}}^{1} dz\,\frac{\theta(1-y^2-z^2)}{\sqrt{1-y^2-z^2}}\mathcal{A}_y[\ln(1+s^2)]\mathcal{A}_z[\ln(1+t^2)] - \int_{-1}^{1} dy\int_0^u d\xi\,\frac{\xi^2}{xR}\ln(1+\sigma^2)\right\}. \tag{A20}$$

Finally, we note that the total imaginary part $W(0,k_f)$ evaluated at zero nucleon-momentum ($q=0$) can even be written in closed analytical form:

$$W(0,k_f) = \frac{g^4 M_N}{16\pi^3}\left\{\frac{\pi^2}{12} + \mathrm{Li}_2(-1-u^2) - \frac{2u^2}{1+u^2} + \left[2 + \ln(2+u^2) - \frac{1}{2}\ln(1+u^2)\right]\ln(1+u^2)\right\}, \tag{A21}$$

where $\mathrm{Li}_2(\ldots)$ denotes the conventional dilogarithmic function. The behavior of $W(0,k_f)$ at small densities is k_f^4.

[1] F. D. Becchetti and G. W. Greenless, Phys. Rev. **182**, 1190 (1969).
[2] R. L. Varner, W. J. Thompson, T. L. McAbee, E. J. Ludwig, and T. B. Clegg, Phys. Rep. **201**, 57 (1991).
[3] A. J. Koning and J. P. Delaroche, Nucl. Phys. A **713**, 231 (2003).
[4] F. M. Nunes and A. Deltuva, Phys. Rev. C **84**, 034607 (2011).
[5] J. P. Jeukenne, A. Lejeune, and C. Mahaux, Phys. Rep. **25**, 83 (1976).
[6] P. Grange, J. P. Cugnon, and A. Lejeune, Nucl. Phys. A **473**, 365 (1987).
[7] W. Haider, A. M. Kobos, and J. R. Rook, Nucl. Phys. A **480**, 1 (1988).
[8] E. Bauge, J. P. Delaroche, and M. Girod, Phys. Rev. C **58**, 1118 (1998).
[9] E. Bauge, J. P. Delaroche, and M. Girod, Phys. Rev. C **63**, 024607 (2001).
[10] M. Hemalatha, Y. K. Gambhir, S. Kailas, and W. Haider, Phys. Rev. C **75**, 037602 (2007).
[11] D. Pachouri, S. Rafi, and W. Haider, J. Phys. G **39**, 055101 (2012).
[12] L. G. Arnold, B. C. Clark, R. L. Mercer, and P. Schwandt, Phys. Rev. C **23**, 1949 (1981).
[13] B. ter Haar and R. Malfliet, Phys. Rep. **149**, 207 (1987).
[14] S. Hama, B. C. Clark, E. D. Cooper, H. S. Sherif, and R. L. Mercer, Phys. Rev. C **41**, 2737 (1990).
[15] G. Q. Li, R. Machleidt, and R. Brockmann, Phys. Rev. C **45**, 2782 (1992).
[16] R. Xu, Z. Ma, E. N. E. van Dalen, and H. Müther, Phys. Rev. C **85**, 034613 (2012).
[17] W. H. Dickhoff and C. Barbieri, Prog. Part. Nucl. Phys. **52**, 377 (2004).
[18] S. J. Waldecker and C. Barbieri, and W. H. Dickhoff, Phys. Rev. C **84**, 034616 (2011).
[19] N. Kaiser, S. Fritsch, and W. Weise, Nucl. Phys. A **700**, 343 (2002).
[20] N. Kaiser, S. Fritsch, and W. Weise, Nucl. Phys. A **750**, 259 (2005).
[21] S. Rafi, M. Sharma, D. Pachouri, W. Haider, and Y. K. Gambhir, Phys. Rev. C **87**, 014003 (2013).
[22] B. S. Pudliner, V. R. Pandharipande, J. Carlson, and R. B. Wiringa, Phys. Rev. Lett. **74**, 4396 (1995).
[23] A. Lejeune, P. Grange, M. Martzolff, and J. Cugnon, Nucl. Phys. A **453**, 189 (1986).
[24] J. S. Bell and E. J. Squires, Phys. Rev. Lett. **3**, 96 (1959).
[25] P. Wang, S.-X. Gan, P. Yin, and W. Zuo, Phys. Rev. C **87**, 014328 (2013).
[26] D. R. Entem and R. Machleidt, Phys. Rev. C **68**, 041001(R) (2003).
[27] D. Gazit, S. Quaglioni, and P. Navrátil, Phys. Rev. Lett. **103**, 102502 (2009).
[28] J. W. Holt, N. Kaiser, and W. Weise, Phys. Rev. C **79**, 054331 (2009).
[29] J. W. Holt, N. Kaiser, and W. Weise, Phys. Rev. C **81**, 024002 (2010).
[30] K. Hebeler and A. Schwenk, Phys. Rev. C **82**, 014314 (2010).
[31] J. W. Holt, N. Kaiser, and W. Weise, Nucl. Phys. A **870–871**, 1 (2011).
[32] J. W. Holt, N. Kaiser, and W. Weise, Nucl. Phys. A **876**, 61 (2012).
[33] N. M. Hugenholtz and L. Van Hove, Physica **24**, 363 (1958).
[34] J. M. Luttinger, Phys. Rev. **121**, 942 (1961).
[35] C. Mahaux and R. Sartor, Phys. Rev. Lett. **57**, 3015 (1986).
[36] J.-P. Jeukenne, A. Lejeune, and C. Mahaux, Phys. Rev. C **16**, 80 (1977).
[37] J. W. Negele and K. Yazaki, Phys. Rev. Lett. **47**, 71 (1981).
[38] S. Fantoni, B. L. Friman, and V. R. Pandharipande, Phys. Lett. B **104**, 89 (1981).